A NOVEL MULTIRESOLUTION-BASED HYBRID APPROACH FOR 3D FOOTWEAR OUTSOLE FEATURE CLASSIFICATION AND EXTRACTION

Bo Gao and Nigel M. Allinson

Department of Electronic and Electrical Engineering
University of Sheffield, Mappin Street, S1 3JD, Sheffield, UK
email: {elp05bg, n.allinson}@sheffield.ac.uk
web: http://www.shef.ac.uk/eee/research/iel

ABSTRACT

Footwear impressions retrieved from crime scenes are often due to shoes in various stages of wear. This forensic-related research on footwear recognition is able to extract information-rich 3D outsole patterns and produce 2D shoeprints regardless of different degrees of wear. Based on pattern characteristics, outsoles are categorized into two types, Convex-Pattern-Dominant Outsoles (Convex-PDOs) and Concave-Pattern-Dominant Outsoles (Concave-PDOs). Initial work for extracting 3D Features from Concave-PDOs is reported in this paper. In our proposed method, outsole models are first captured using a 3D scanner. Patterns corresponding to higher and lower curvature variations are subsequently classified using a multiresolution-based curvature analysis approach. In a subsequent step to discard outliers from the extracted 3D features, by modifying contours of 3D outsole models, a pyramid method is employed to generate composite results. Visual analysis on current experimental investigations shows promising results for further 3D feature extraction and 2D shoeprint generation.

1. INTRODUCTION

Crime scene analysis has traditionally employed biometric evidence such as fingerprints, hair and DNA samples. However, compared to conventional biometric modalities, it is often harder for a suspect not to leave traces of their shoeprints on the ground or other surfaces. Therefore, in absence of strong biometric evidence, footwear impressions are possibly the only clue in identifying a suspect [1], and also potentially provide key intelligence to other crimes. Furthermore, shoeprint impressions have even higher capture possibility than fingerprints under specific situations [1]. Research by Alexandre [2] shows that approximately 30% of shoeprints left at burglary crime scenes are likely to be employed for further investigation. Due to its advantages in forensic investigations, footwear recognition has become a recently highlighted research topic in forensic science.

2. RELATED WORK

Currently to accelerate footwear matching procedures, research in this area mainly focuses on developing automated footwear recognition systems. In the early work reported by Geradts and Keijzer [3], primitive morphology operators are employed to encode geometric shapes in each outsole pattern. The spatial locations and frequency of these shapes are classified by artificial neural networks. However, no experimental results are reported by the authors. In a later approach, reported in [4, 5], fractal and mean square noise error are employed for shoeprint pattern representation and matching criteria respectively. The proposed system was tested for 145 outsole patterns with no rotational and scale variations and a system accuracy of 88% was reported. In [6], by encoding the spatial frequencies, Fourier Transforms are used for the matching of full and partial shoeprints, and provide a degree of translational and rotational invariance. Reference patterns are sorted in a descending order according to their resemblance to the query image. In the sorted database, authors report that, for full-prints, the scores of correctly matching the first and the first 5% of reference patterns to the query image are 65% and 87% respectively. The same evaluations are also carried out on partial-prints and lead to 55% and 78% of matching respectively. More recently, automated shoeprint recognition system utilizing both feature detectors/descriptors and spectral correspondence is also reported in [7]. In the proposed algorithm, features are first extracted from shoeprint patterns by a Maximally Stable Extremal Region (MSER) detector and subsequently described by a Scale Invariant Feature Transform (SIFT) descriptor. After a coarse-level matching, a shorter list is retained for a finer search in which shoeprints are compared according to their constrained spectral correspondence. The system works with a reference database accommodating 374 shoeprints and delivers 87% first-rank and 92% top-eight ranked performance.

Even though skilled techniques were comprehensively used in the work reviewed above, the matching processing is carried out on 2D synthesized shoemarks only. (More recently, analysis of 2D shoemarks coming from real crime scenes has been reported in [8].) Such a fact leads to significant performance degradation while tackling shoeprints left by outsoles with different degrees of abrasion. However, for current systems, solutions such as including several shoeprints of the same outsole in different wear states in the database seem to be practical options, but only a limited number of samples are infeasible to cover the whole wear cycle. Therefore, a footwear matching system capable of using 3D depth information to produce 2D shoeprint based on expected abrasion is very likely to be an encouraging solution. Whereas, due to irregularity represented in both outsole contours and patterns, it is more reliable to classify outsoles into

 ISSN 2076-1465

several typical categories and produce an extraction scheme according to each type. In our previous work [9], based on outsole pattern characteristics, outsoles are categorized into two types – *Convex-Pattern-Dominant Outsoles* (*Convex-PDOs*, such as the shoe shown in Fig. 1(a)) and *Concave-Pattern-Dominant Outsoles* (*Concave-PDOs*, such as the shoe shown in Fig. 1(b)). To classify concave and convex features on the outsole pattern, a parabolic model is first applied to estimate each baseline contour along the width direction. Concave and convex features on each baseline are subsequently classified by a Gaussian-like kernel model. Eventually, for *Convex-PDOs*, a fuzzy c-mean based approach is also reported for extracting *Printable 3D Features* (Definition given in the Section 3.2). Though promising results have been produced for *Convex-PDOs*, this model-based method cannot provide reliable performance when dealing with *Concave-PDOs*. Compared to depth difference between convex and concave features on *Convex-PDOs*, which is normally about several mm, the counterpart on *Concave-PDOs*, as shown in Fig. 1(c), downgrades to the level of 10^{-1} mm, which makes our model-based approach very vulnerable to noise. Thereby, to extract *Printable 3D Features* from *Concave-PDOs*, a novel multiresolution-based hybrid method is proposed in this paper.

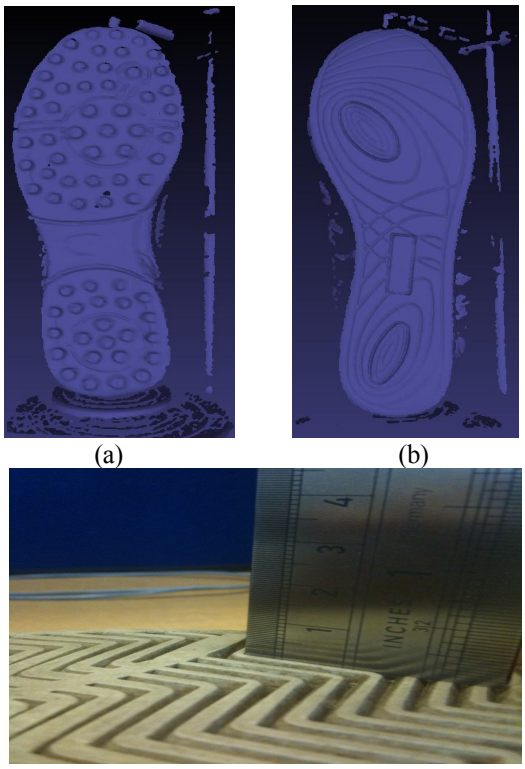

(a) (b)

(c)

Figure 1 (a) and (b) Outsole models captured by 3D scanner; (c) Feature depth in the level of 10^{-1} mm.

3. PROPOSED APPROACH

3.1 3D Outsole Model Capture and Modification

In our approach, 3D outsole models are first captured by a 3D laser scanner and saved as obj files, shown in Fig. 1(a) and (b). Currently, the scanning resolution is set to 400 dpi. The triangles with side lengths of 0.38 – 1.14 mm are applied for meshing scanned models. The operating distance between a shoe and the scanner is set to about 380 mm in order to capture the whole contours of shoes in the maximum size of 10 (UK standard; 44.5 European; 10.5 US). After manually removing redundant margins, polygon-meshed models are further converted to rectangular-grid format at 0.25 mm resolution for further manipulation.

3.2 Multiresolution-Based Curvature Analysis

To artificially produce 2D shoeprints based on relevant 3D outsole models, 3D features capable and incapable of leaving 2D prints on a flat surface are first classified into two types, *Printable 3D Features* and *Unprintable 3D Features*. Then, due to composition duality of 3D feature types, successful extraction for either type of 3D features results in entire knowledge of the other. Based on distinct shape formations owned by each type of 3D features and dramatic shape distortions observed on conjunctional areas of them, it is rational to believe that, for *Concave-PDOs*, *Printable* and *Unprintable 3D Features*, in general, have lower and higher extrinsic curvature values respectively. Thus, curvature analysis becomes an ideal way to implement classification.

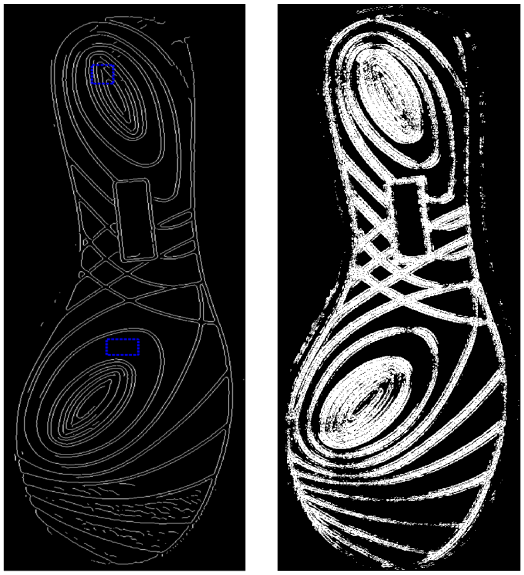

(a) (b)

Figure 2 In the edge map (a), marked rectangles are setup by users for centroid initialization. (b) Result produced by multiresolution-based curvature analysis operations. Dark and white indicate *Printable* and *Unprintable 3D Features* respectively.

As a concept able to describe bending of a geometrical shape, curvature is frequently used for surface segmentation and smoothing [10, 11]. To estimate curvature values over triangulated meshes, two major approaches are proposed, which are an analytic approach and a discrete approach. The analytic approach focuses on calculating curvature values of meshed vertices interpolated by smooth functions [12, 13] and generally performs well, but is computationally intensive. It is hence not an ideal option for our large-size 3D outsole

models. The discrete approach, by applying the discretisation of derivatives of the Gauss-Bonnet formula, approximates curvature values of each vertex. Several useful curvature approximations are proposed in [14, 15]. Whereas, calculation of all of them depends on their neighbourhoods, and thus are error-prone when the neighbourhood-oriented normalization factor is extremely small. Thereby, concentrated curvature, a concept giving a neighbourhood-independent approximation of Gaussian curvature, is introduced in [16]; and utilized for curvature estimation on our 3D outsole models. To calculate the concentrated curvature at point *c*, the neighbourhood of this point needs to be divided into eight triangles, each of which is composed by point *c* and its two adjacent neighbouring points. The concentrated curvature K_c at point *c* is then defined by

$$K_c = 2\pi - \sum_{i=1}^{N=8} \theta_i \qquad (1)$$

$$\theta_i = \arcsin\left(\frac{|v_i \times v_{i+1}|}{|v_i| \bullet |v_{i+1}|}\right) \qquad (2)$$

Where θ_i is the angle of an incident triangle at point *c*. v_i and v_{i+1} are vectors deriving from point *c* and pointing to its two adjacent neighbour points.

To produce unambiguous 2D shoeprints, it is best to extract either type of 3D features with spatial distributions as continuous as possible; in other words, containing isolated points as less as possible. The current approach, however, for calculating the concentrated curvature of each point over its immediate neighbourhood is still vulnerable to noise and it is easy to generate isolated points. Hence, instead of defining both types of 3D features in terms of their pure curvature values, curvature variation due to resolution changes are used for 3D feature classification. It is easy to assume that, for a point included by a relatively flat surface, its curvature values calculated by equation (1) are stable for all resolution settings. However, for a point inside a surface encapsulating high curvature components, its curvature under different resolutions tend to be unpredictable. Therefore, if we define the 1st order neighbourhood as that of being one step away from the target point, the 2nd order neighbourhood as that two steps away from the target point, and so on; the absolute difference between curvature values computed based on neighbourhoods in two different orders is used to evaluate the curvature on each point in the 3D outsole model. Robustness of this multiresolution-based approach has been tested in our implementation. Normally, for curvatures calculated upon 1st and 4th order neighbourhoods, curvature variations of points from the type of *Unprintable 3D Features* stay in the level of 10^{-1} ~10^{-2}, whereas those from the type of *Printable 3D Features* hold curvature variations in the magnitude order of 10^{-4}~10^{-5}. Due to dramatic differences in curvature variations represented by both types of 3D features, a centroid-based method is used in our implementation. For both types of 3D features, a centroid indicating the standard curvature variation within each category is defined. Points with curvature variations having closer Euclidean distances to a certain centroid are categorized as the relevant type. At present, the automated algorithm for discovering centroid values is still under investigation, so in our current implementation, initialization on such values relies on user input. To define values for these two centroids, in each outsole models, users are expected to select two rectangular regions, in each of which a majority of elements belong to a desired type. In the example shown in Fig. 2(a), rectangular regions marked at the bottom and top are those for setting up centroids of *Printable* and *Unprintable 3D Features* respectively. Eventually, centroids are set as mean values of curvature variations in both selected areas. The classification result for the outsole pattern shown in Fig. 1(b) is presented in Fig. 2(b) in which *Printable* and *Unprintable 3D Features* are marked in dark and white notation. It is obvious that, at the end of the processing, the majority of *Unprintable 3D Features* are extracted, but, due to high curvature variations occurring on conjunctional regions (edges) between two types of 3D features, a large amount of outliers on edges are also included. Outliers are of great potential to degrade 2D shoeprints finally retrieved, especially when outsole surfaces own compact patterns such as concentric rings shown in Fig. 2(b).

3.3 Pyramid Method for 3D Model Contour Modification

To remove outliers from *Unprintable 3D Features*, a classification approach based on their depth difference is regarded as a solution. But it is of infeasibility to apply this approach directly on 3D outsole models, due to their highly-bended contours. For the shoe model in Fig. 1(b), the extreme depth values are 108.79 units and 67.63 units. The standard deviation is also 8.96 units, however actual maximum depth difference within *Unprintable 3D Features* (ridges) is about 1 unit. Therefore, for each outsole model, before discarding outliers, it is essential to attain a basic contour with a depth variance lower than that within *Unprintable 3D Features.*

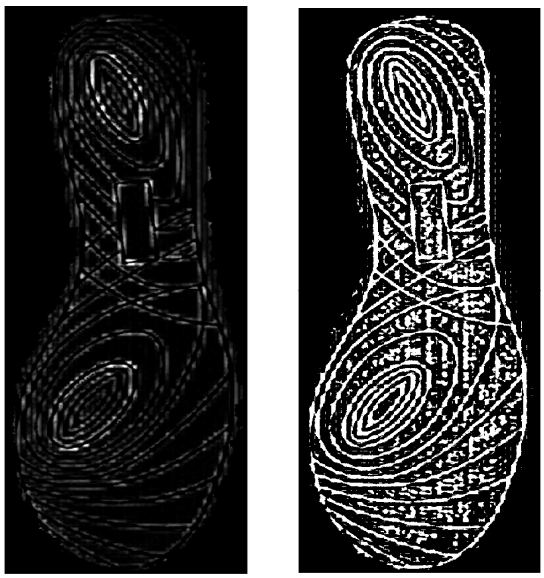

(a) (b)

Figure 3 (a) The reconstructed result (b) The reconstructed result after threshold (0).

If we examine the problem in the frequency domain, it is easy to find out that *Unprintable 3D Features* contain high frequency signals. Therefore, an approach capable in suppressing low frequency signals is required. In our implementation, a 4-leveled pyramid method is used for bandpass filtering. For each outsole, four grid-meshed models in different resolutions are first produced. The scale factor between successive resolutions is two. To create model contours excluding low frequency signals, the pyramid deconstruction processing is first carried out between each adjacent level. This processing is described by equation (3) - (5), in which *sf* is the scale factor equal to 2, $I(\bullet)$ is the interpolation operation, and *m* indicate models in different resolutions. The deconstruction manipulation yields three difference components, $\Delta_{1\sim3}$ in which bandpassed frequencies rank in a descending order. Even though low frequency signals are successfully removed in each level, *Unprintable 3D Features* also entail some loss of information in each level of deconstruction. Therefore, to obtain *Unprintable 3D Features* which retain as much fidelity as possible to the original, the deconstruction results are eventually combined together. This processing is called reconstruction and defined by equation (6)-(7).

$$\Delta_1 = m_1 - I(m_2, sf) \qquad (3)$$

$$\Delta_2 = m_2 - I(m_3, sf) \qquad (4)$$

$$\Delta_3 = m_3 - I(m_4, sf) \qquad (5)$$

$$r_2 = \Delta_2 + I(\Delta_3, sf) \qquad (6)$$

$$r_1 = \Delta_1 + I(r_2, sf) \qquad (7)$$

The reconstruction result of the shoe model in Fig. 1(b) is displayed in Fig. 3(a), in which overall maximum and minimum values downgrade to 1.52 and -2.22 units. The overall standard deviation is also reduced to 0.22 units, whereas the actual maximum depth difference within *Unprintable 3D Features* remains in about 1 unit. Moreover, as another advantage of this approach, enhanced edges contributing to clear contours of *Unprintable 3D Features* are also shown. Even though in the reconstructed model, two types of 3D Features have shared depth ranges, they are well-divided by enhanced edges. Hence, by defining a global threshold lower than edges, segmentation can be achieved. So far, the global threshold is crude and set as 0. The result after thresholding is shown in Fig. 3(b), in which two types of 3D Features are well-segmented, albeit both of them are displayed. Eventually, *Unprintable 3D Features* are defined as those extracted by the curvature analysis process with reconstruction results lower than the global threshold. The final extraction result is shown in Fig. 4(a).

4. EXPERIMENTS

To benchmark the capability of our extraction algorithm, effectively presented by running our results with a footwear recognition system is the best way, however, systems reviewed previously are all designed for grayscale shoeprint images. Therefore, to fulfil justified evaluations, an interface

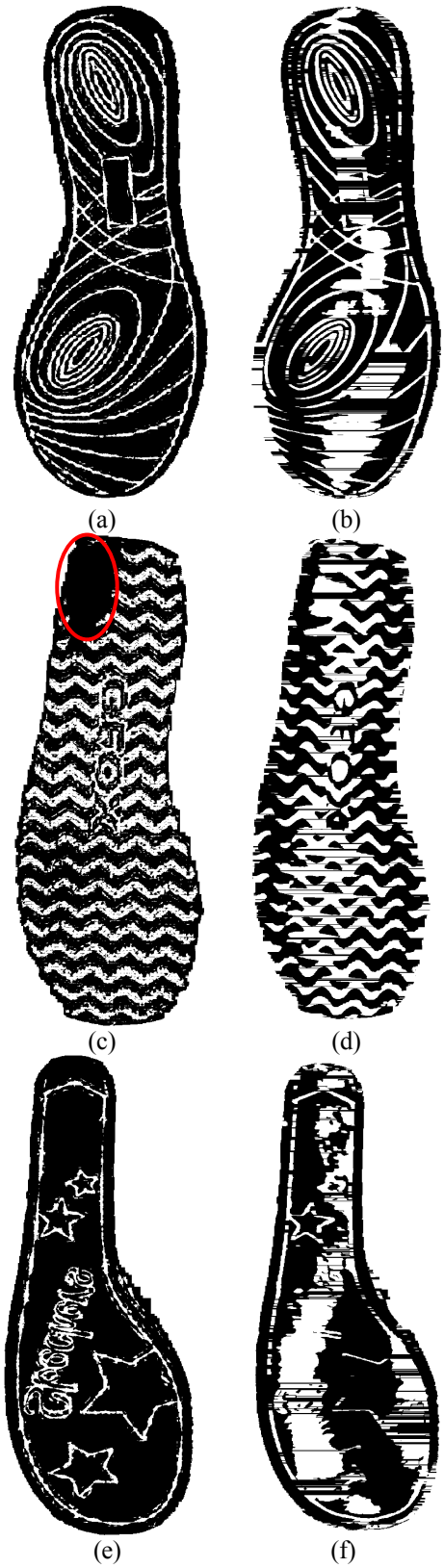

Figure 4. (a), (c) and (e) are 2D shoeprints produced by our proposed algorithm. In (c), a worn-out feature is circled. (b), (d) and (f) are 2D shoeprints produced by our previous method [8].

for current shoeprint recognition systems is under investigation. In this paper, three extraction results, in Fig. 4(a), (c) and (e), are presented to compare with those, in Fig. 4(b), (d), and (f), obtained by our previous method [9]. In all these three experiments, the curvature variations are calculated based on 1st and 4th order neighbourhoods. The triangle size, in model capture stage, is set as 1.14 mm for first two experiments, and 0.38 mm for the last one (due to slim ridges in the outsole pattern).

It is obvious that our proposed algorithm produces better results than our previous work. Even though, our current results still contain a limited number of artefacts, they are randomly distributed in the spatial domain. Compared to the fully-connected regional noises shown in Fig.4(b), (d), and (f), these isolated noise artefacts with random distributions tend to incur with a much less effect for further pattern matching. Except the low noise rate, our proposed algorithm is more capable of discovering pattern details. In Fig. 4(c), the 2D shoeprint produced by our proposed method not only succeeds in presenting wave-like patterns but also captures a worn-out feature marked by a circle in the figure. Such a merit guarantees system robustness when tackling worn footwear.

5. CONCLUSION AND FURTHER WORK

In this paper, a multiresolution-based hybrid approach for 3D outsole feature classification and extraction is reported. To produce 2D shoeprint, 3D features are first defined as *Printable* and *Unprintable* ones based on their contribution to 2D impressions. Two multiresolution-based methods are subsequently employed for curvature and frequency domain analysis. Eventually, feature classification and extraction are achieved by combining both analysis results together. To refine current results, our further work will focus on noise removal. Work to design an interface for adapting our result to current grayscale image-based shoeprint recognition system will also be examined. Eventually, by including our previous algorithm for *Convex-PDOs* [9], a unified solution is expected to solve generic outsole patterns.

REFERENCES

[1] W. J. Bodziak, “Footwear impression evidence detection, recovery and examination, Second Edition”, CRC Press, Boca Raton, Florida, 2000.

[2] G. Alexandre, “Computer Classification of the Shoeprint of Burglar Shoes”, Forensic Science International, 1996, Volume 82: 59-65.

[3] Z. Geradts and J. Keijzer, “The image-database REBEZO for shoeprints with developments on automatic classification of shoe outsole designs”, Forensic Science International., 1996, Volume 82, pp. 21-31.

[4] A. Bouridane, A. Alexander, M. Nibouche and D. Crookes, “Application of fractals to the detection and classification of shoeprints”, Proc. 2000 Int'l Conf. Image Processing, Vancouver, BC, Canada, 2000, vol. 1, pp. 474-477

[5] A. Alexander, A. Bouridane and D. Crookes, “Automatic classification and recognition of shoeprints”, Proc. Seventh Int. Conf. Image Processing and Its Applications, University of Manchester, UK, 1999, vol 2, pp. 638-641

[6] P. De Chazal, J. Flynn, and R. Reilly, ”Automated processing of shoeprint image based on the fourier transform for use in forensic science”, IEEE Trans. Pattern Analysis Machine Intelligence, 27, 2005, pp. 341–350.

[7] M. Pavlou and N. Allinson, “Automated encoding of footwear patterns for fast indexing”, Image Vision Computing, 27, 2009, pp. 402–409.

[8] F. Dardi, F. Cervelli, and S. Carrato, ”An automatic footwear retrieval system for shoe marks from real crime scenes”, in *Proc. ISPA 09*, Salzburg, Austria, September 16-18. 2009, pp. 668-672

[9] B. Gao and N. Allinson, “A novel model-based approach for 3D footwear outsole feature extraction”, in *Proc. ISPA 09*, Salzburg, Austria, September 16-18. 2009, pp. 673-677

[10] A. Mangan and R. Whitaker, “Partitioning 3D surface meshes using watershed segmentation”, IEEE Transaction on Visualization and Computer Graphics, 1999, 5(4):308–321.

[11] D. L. Page, A. Koschan, and A. Abidi, “Perception-based 3d triangle mesh segmentation using fast marching watersheds”, In IEEE Computer Society Conference on Computer Vision and Pattern Recognition, volume 2. IEEE Computer Society, 2003.

[12] N. A. Nabih, “Algebraic error analysis for surface curvatures and segmentation of 3d range images”, Pattern Recognition, 23, 1989, pp. 807–817.

[13] E. M. Stokely and S. Y. Wu, “Surface parametrization and curvature measurement of arbitrary 3-d objects: Five pratical methods”, IEEE Transactions on pattern analysis and machine Intelligence, 1992, pp. 833–839.

[14] M. Meyer, M. Desbrun, P. Schroder, and A. Barr, “Discrete differential-geometry operator for triangulated 2-manifolds”, In Proceedings of VisMath’02, Berlin, Germany, 2002.

[15] T. D. Gatzke and C. M. Grimm, “Estimating curvature on triangular meshes”, International Journal on shape Moedeling, 12(1), 2006, pp.1–29.

[16] M. Troyanov, “Les surfaces euclidiennes a singularit´es coniques”, L’Enseignement Math´ematique, 32, 1986, pp. 79–94.